Regional temperature change potentials for short-lived climate forcers based on radiative forcing from multiple models

Atmos. Chem. Phys., 17, 10795–10809, 2017
https://doi.org/10.5194/acp-17-10795-2017

Atmospheric Chemistry and Physics
Open Access
EGU

Regional temperature change potentials for short-lived climate forcers based on radiative forcing from multiple models

Borgar Aamaas[1], Terje K. Berntsen[1,2], Jan S. Fuglestvedt[1], Keith P. Shine[3], and William J. Collins[3]

[1]CICERO Center for International Climate Research, PB 1129 Blindern, 0318 Oslo, Norway
[2]Department of Geosciences, University of Oslo, Oslo, Norway
[3]Department of Meteorology, University of Reading, Reading RG6 6BB, UK

Correspondence to: Borgar Aamaas (borgar.aamaas@cicero.oslo.no)

Received: 14 February 2017 – Discussion started: 14 March 2017
Revised: 5 July 2017 – Accepted: 14 August 2017 – Published: 14 September 2017

Abstract. We calculate the absolute regional temperature change potential (ARTP) of various short-lived climate forcers (SLCFs) based on detailed radiative forcing (RF) calculations from four different models. The temperature response has been estimated for four latitude bands (90–28° S, 28° S–28° N, 28–60° N, and 60–90° N). The regional pattern in climate response not only depends on the relationship between RF and surface temperature, but also on where and when emissions occurred and atmospheric transport, chemistry, interaction with clouds, and deposition. We present four emissions cases covering Europe, East Asia, the global shipping sector, and the entire globe. Our study is the first to estimate ARTP values for emissions during Northern Hemisphere summer (May–October) and winter season (November–April). The species studied are aerosols and aerosol precursors (black carbon, organic carbon, SO_2, NH_3), ozone precursors (NO_x, CO, volatile organic compound), and methane (CH_4). For the response to BC in the Arctic, we take into account the vertical structure of the RF in the atmosphere, and an enhanced climate efficacy for BC deposition on snow. Of all SLCFs, BC is the most sensitive to where and when the emissions occur, as well as giving the largest difference in response between the latitude bands. The temperature response in the Arctic per unit BC emission is almost four times larger and more than two times larger than the global average for Northern Hemisphere winter emissions for Europe and East Asia, respectively. The latitudinal breakdown likely gives a better estimate of the global temperature response as it accounts for varying efficacies with latitude. An annual pulse of non-methane SLCF emissions globally (representative of 2008) lead to a global cooling. In contrast, winter emissions in Europe and East Asia give a net warming in the Arctic due to significant warming from BC deposition on snow.

1 Introduction

Climate is influenced by a multitude of emissions with varying impacts (e.g. Myhre et al., 2013). Emissions of short-lived climate forcers (SLCFs), such as black carbon (BC), organic carbon (OC), SO_2, NH_3, NO_x, CO, and volatile organic compounds (VOCs), affect the composition of the atmosphere primarily on timescales of days to a few months. CH_4 is included in the definition because its lifetime of around 10 years is shorter than timescales for stabilizing the climate (Aamaas et al., 2016). The variation in the geographical pattern of SLCF emissions has changed over time, with emissions typically being high in the early phases of industrialization, and then gradually being reduced due to air quality concerns and technological improvements. Nevertheless, emissions are still growing in many parts of the world, and there is a growing focus politically to develop a mitigation strategy for the SLCFs to achieve both improved air quality and slowing global warming (Schmale et al., 2014; Shindell et al., 2012; Stohl et al., 2015).

Due to the short atmospheric lifetimes, emissions of SLCFs lead to a spatial pattern in radiative forcing (RF) that is more inhomogeneous than for emissions of long-lived greenhouse gases such as CO_2. While we focus on RF from large emission regions, Bowman and Henze (2012) and Henze et al. (2012) showed that radiative forcing efficiencies

can vary by 1000 % for much smaller emission regions. It is well established that there is not a close relationship between the RF pattern and the surface temperature response pattern, due to modifications by heat transport in the atmosphere and ocean and the spatial variability in climate feedbacks (e.g. Boer and Yu, 2003). However, as shown by Shindell and Faluvegi (2009) and Shindell (2012), it is possible to establish relationships between the RF pattern caused by a certain constituent and the response in broad latitude bands. Recently, Najafi et al. (2015), have shown from observational and model data that there is a distinct difference in the Arctic response to the overall forcing by ozone, aerosols, and land use compared to other latitude bands.

Emission metrics are simple tools based on comprehensive model simulations that relate emissions to a certain response (physical climate change or economic damage), e.g. Fuglestvedt et al. (2003) and Tol et al. (2012). The most widely used emission metric, the global warming potential (GWP), is given by the integrated RF (over a time horizon of H years) in response to a pulse emission. Shine et al. (2005) introduced the Global Temperature Change Potential (GTP) using the surface temperature change (after a time horizon of H years) for the response. Emissions metrics have typically estimated a global effect due to global emissions (e.g. Aamaas et al., 2013). A first step going beyond global means was to quantify the global response based on regional emissions for SLCFs (Fuglestvedt et al., 2010; Collins et al., 2013; Aamaas et al., 2016). By introducing the concept of regional temperature potentials (RTPs), Shindell and Faluvegi (2010) extended the metric concept to include regional responses (in terms of surface temperature change in broad latitude bands) from regional RFs.

In addition to the regionality, the timing of the SLCFs emissions matter. This is potentially important, since the photochemistry in the atmosphere, lifetime, atmospheric transport, and forcing efficiency is likely to vary between the seasons. As some sources (e.g. domestic heating and agricultural waste burning) have a large seasonal cycle, using seasonal RTP metrics might have a significant impact on the evaluation of cost effectiveness of mitigation measures.

Here we use detailed multimodel calculations of the relationship between emission location and the resulting specific RF (RF per Tg yr^{-1} emissions) for SLCFs (Bellouin et al., 2016; Sect. 2.1) and the regional climate sensitivities (e.g. Shindell and Faluvegi, 2009) to estimate ARTPs for a range of aerosols, aerosol precursors, and ozone precursors (BC, OC, SO_2, NH_3, NO_x, CO, and VOC), and CH_4 (Sect. 2.2). The findings mostly confirm the results by Collins et al. (2013) and extend the global temperature responses estimated by Aamaas et al. (2016) to responses on latitude bands. Our study is the first to calculate ARTPs for NH_3 emissions. The treatment of BC in the Arctic is more complex, which has a high influence on the ARTPs for BC. Aspects of the aerosol effects on ozone precursors are also novel. For the first time, we distinguish between ARTPs for emissions taking place during Northern Hemisphere (NH) summer (May–October) and winter (November–April). ARTP metrics are calculated for regional emissions from Europe, East Asia, and the shipping sector, as well as for global emissions (Sect. 3.1). The ARTP values are applied to calculate regional temperature responses of global emissions in Sect. 3.2. We also make a comparison of ARTPs with AGTPs (Sect. 3.3). Uncertainties are discussed in Sect. 3.4, and we conclude in Sect. 4.

2 Material and methods

2.1 Radiative forcing

The RFs that are the basis for the ARTP calculations of the SLCFs are calculated using four different chemistry climate models or chemical-transport models presented by Bellouin et al. (2016); see details about the models in Table 1. RFs are produced based on a control simulation and numerous perturbation simulations that consider a 20 % emission reduction in one type of species and one region in NH summer or winter. The ECLIPSE emission data set applied here was created with the GAINS (Greenhouse Gas – Air Pollution Interactions and Synergies) model; see Stohl et al. (2015). The regional RFs are then averaged for four latitude bands, southern middle–high latitudes (90–28° S), the tropics (28° S–28° N), northern midlatitudes (28–60° N), and the Arctic (60–90° N), as forcing-response coefficients are only available for those latitude bands in the literature (e.g. Shindell and Faluvegi, 2010; Shindell, 2012).

We compute ARTPs for six different effects that contribute to the RF for each species (aerosol effects, BC deposition on snow, BC semi-direct, short-lived ozone, methane, and methane-induced ozone). The quantification of these effects are given by the RF data from Bellouin et al. (2016). For the general circulation models, the RFs of the aerosol perturbations are calculated online using two calls to the radiation scheme. This method involves diagnosing radiative fluxes with and without the perturbation. These RFs do not include rapid adjustments (even in the stratosphere). For the OsloCTM2 chemistry transport model and the RF exerted by the ozone precursors in all the models, RF is computed by offline radiative transfer codes. The RF for methane is based on the analytical expression that includes stratospheric adjustments (Myhre et al., 1998), which gives a global mean. Based on this global RF estimate, we apply the latitudinal pattern in RF for methane and methane-induced ozone response in Collins et al. (2013). This pattern is based on an ensemble of 11 global chemical transport models that evaluated a global reduction of CH_4 mixing ratio, where RF was calculated using the method developed by the NOAA Geophysical Fluid Dynamics Laboratory (Fry et al., 2012).

For aerosols and aerosol precursors, all four models calculate the aerosol direct and first indirect (cloud-albedo) ef-

Table 1. The models and species included. Models are either general circulation models (GCM) or chemistry transport models (CTM). The resolution column shows the horizontal resolution and the number of vertical layers.

Model	Type	Resolution	BC	OC	SO_2	NH_3	NO_x	CO	VOC	CH_4	References
ECHAM6-HAMMOZ	GCM	1.8° × 1.8° L31	×	×	×						Stevens et al. (2013)
HadGEM3-GLOMAP	GCM	1.8° × 1.2° L38	×	×	×		×	×	×	×	Hewitt et al. (2011)
NorESM	GCM	1.9° × 2.5° L26	×	×	×		×	×	×	×	Bentsen et al. (2013), Iversen et al. (2013)
OsloCTM2	CTM	2.8° × 2.8° L60	×	×	×	×	×	×	×	×	Søvde et al. (2008), Myhre et al. (2009)

fect, except ECHAM6 which only includes direct RF. In this study, we group together the aerosol direct and first indirect (cloud-albedo) effect and name this "aerosol effects". In addition, OsloCTM2 estimated the RF from BC deposition on snow and the semi-direct effect. The semi-direct effect is quantified in Bellouin et al. (2016) by prescribing control and perturbed distributions of BC mass-mixing ratios based on OsloCTM2 in 30-year, fixed sea-surface simulations with the Community Earth System Model (CESM). The RF from aerosol–radiation interactions was quantified with multiple calls to the radiation scheme. Because the semi-direct effect is not included in the CAM4 component of the CESM, the semi-direct effect is calculated as the difference between the RF from aerosol–radiation interactions and the effective RF. For the ozone precursors and CH_4, the total RF takes into account the aerosol direct and first indirect effects, short-lived ozone effect, methane effect, and methane-induced ozone effect. The ozone precursors and CH_4 can influence the aerosol effects, as a reduction in CH_4 concentration leads to increase in OH, which promotes sulfate aerosol formations. Only OsloCTM2 includes an estimate for nitrate aerosols, which is added to the aerosol effect quantification in the other models.

The best estimate of a species' RF has been calculated as the sum of all effects in which the average across the models is used for each effect. Not all models have estimated RFs for all species and effects. In addition, ECHAM6 is excluded from the best estimates for BC, OC, and SO_2, since it did not estimate the first indirect effect. For BC deposition on snow, the BC semi-direct effect, and nitrate aerosol, the best estimate is solely based on the OsloCTM2 model, while the best estimates are based on three models for all other effects (aerosol effects, short-lived ozone, methane, and methane-induced ozone).

For the high and low estimates of RF for each emission case, we find these values by taking the sum of the highest and lowest values, respectively, from all models for each individual effect.

The emission regions are defined according to tier1 Hemispheric Transport of Air Pollution (HTAP) regions (see Bellouin et al., 2016). Europe is defined as western and eastern Europe up to 66° N including Turkey. East Asia includes China, Korea, and Japan. Shipping is the global shipping sector. The global emissions category excludes this shipping activity. As RF values are also available for the remaining land areas outside of Europe and East Asia, results from the rest of the world are presented in Sect. S2.

2.2 Regional temperature change potentials

The regional temperature response has been calculated on the basis of RF in the latitude bands and regional climate sensitivities, as well as the temporal evolution of an idealized temperature response. Even though our estimates are based on seasonal emissions, the temperature responses calculated are annual means. The general expression for the ARTP following a pulse emission of constituent i (E_i) in region r which leads to a response in latitude band m is as follows (e.g. Collins et al., 2013):

$$\mathrm{ARTP}_{i,r,m,s}(H) = \sum_{l} \int_{0}^{H} \frac{F_{l,i,r,s}(t)}{E_{i,r,s}} \times \mathrm{RCS}_{i,l,m} \times R_{\mathrm{T}}(H-t)\,\mathrm{d}t. \quad (1)$$

$F_{l,r,s}(t)$ is the RF in latitude band l due to emission in region r in season s as a function of time (t) after the pulse emission $E_{r,s}$ (in Tg). Our study differentiates between four latitude response bands, in line with the typical width of response bands to inhomogeneous forcing found by Shindell et al. (2010), while more detailed modelling will be possible with a finer-masked RCS matrix available. The $\mathrm{RCS}_{i,l,m}$ is a matrix of regional response coefficients based on the RTP concept (unitless; see Collins et al., 2013). As these response coefficients are normalized here, they contain no information on climate sensitivity, only the relative regional responses in the different latitude bands. The global climate sensitivity is included in the impulse response function R_{T}, which is a temporal temperature response to an instantaneous unit pulse of RF (in $\mathrm{K\,m^2\,W^{-1}}$). We assume that the time evolution of temperature in each response band follows the global-mean time evolution. Cherubini et al. (2016) show that this simplification is problematic for the first 5–10 years after emissions, but leads to less uncertainty after 20 years, which is our focus. We base our temperature response on that of the HadCM3 climate model (Boucher and Reddy, 2008) with an equilibrium climate sensitivity of $1.06\,\mathrm{K\,m^2\,W^{-1}}$, which translates to a 3.9 K warming for a doubling of CO_2 concentration. This is the same climate sensitivity as for our Absolute Global Temperature Change Potential (AGTP) calculations on the same RF data set (Aamaas et al., 2016).

Regional temperature responses at time t of an emission scenario $E(t)$ can be calculated with these ARTP values by a convolution (see also Aamaas et al., 2016). The temperature response is as follows:

$$\Delta T_{i,r,m,s}(t) = \int_0^t E_{i,r,s}(t') \times \mathrm{ARTP}_{i,r,m,s}\left(t - t'\right) \mathrm{d}t'. \quad (2)$$

2.2.1 For species with lifetimes less than 1 year

For SLCFs with atmospheric lifetimes (or indirect effects causing RF) much shorter than both the time horizon of the ARTP and the response time of the climate system (given by the time constants in R_T above), the general expression for the ARTP can be simplified to the following (see Appendix 2 in Fuglestvedt et al., 2010):

$$\mathrm{ARTP}_{i,r,m,s}(H) = \sum_l \frac{F_{l,i,r,s}}{E_{i,r,s}} \times \mathrm{RCS}_{i,l,m} \times R_\mathrm{T}(H). \quad (3)$$

$F_{l,r,s}$ is the RF over a year where emissions of constituent i ($E_{i,r,s}$ in Tg yr^{-1}) in emission region r occur during season s, either during NH summer or winter.

2.2.2 For species that affect methane

Methane has an adjustment time comparable to the time horizon of the ARTP and the response time of the climate system. So, for species that affect methane, an additional impulse response function that describes the atmospheric decay of methane must be included (R_F). In this case, we add such a function, which governs the methane and methane-induced ozone effects for the ozone precursors (NO_x, CO, and VOC) and CH_4.

$$R_F(t) = e^{-t/\tau}, \quad (4)$$

where $\tau = 9.7$ yr is the average adjustment time for methane in the three models (see Table 7 in Bellouin et al., 2016). If we used the adjustment time of 12.4 yr from Myhre et al. (2013), the ARTP values would be larger. For these species, this additional temperature perturbation due to these effects has to be included:

$$\mathrm{ARTP}(R_F\,\mathrm{response})_{i,r,m,s}(H) = \sum_l \int_o^H \frac{F_{l,i,r,s}}{E_{i,r,s}} \times R_F(H) \times \mathrm{RCS}_{i,l,m} \times R_\mathrm{T}(H-t)\mathrm{d}t. \quad (5)$$

2.2.3 Forcing-response coefficients

The unitless regional sensitivity matrix ($\mathrm{RCS}_{i,l,m}$) is estimated based on literature values of regional response coefficients in K m^2 W^{-1}) (see Sect. 1 in the Supplement for tabulated coefficients). All these response coefficients from the different literature sources have been normalized to the global response in those studies. While the specific regional response coefficients have been estimated in other studies based on climate sensitivities, the normalization to the global response removes the implicit climate sensitivities in the RCS values. We apply several adjustments and refinements of the RCS values (see this section and Sect. 2.2.4): in each case, we normalize the response coefficients and make sure that the climate sensitivity in our ARTP calculations is only included in one of the parameters, in the temporal temperature response (R_T).

As such, RCS matrices only exist for annual emissions, so we assume we can apply the same set of matrices for emissions during NH summer and winter. This assumption is a simplification, but is done implicitly when the annual mean RCS are applied to seasonal varying sources, e.g. wood-burning heating stoves. We believe that calculating explicitly the RF from each season improves the overall ARTP values. For the scattering aerosols and aerosol precursors (SO_2, OC, NH_3), we use the coefficients tabulated in Shindell and Faluvegi (2010), which are the mean responses of CO_2 and SO_2. The same values are used for the longer-lived effects (methane and methane-induced ozone) of the ozone precursors and CH_4. For the short-lived effects of the ozone precursors and CH_4, we apply the O_3 coefficients in Shindell and Faluvegi (2010) as tabulated in Collins et al. (2013).

For BC, the regional sensitivity matrix applied is more complex, and the details for the Arctic-to-Arctic responses are described in Sect. 2.2.4. For other latitude bands, the matrix for the BC aerosol effects is given by BC forcing-response coefficients from Shindell and Faluvegi (2009) as tabulated in Table 3 in Collins et al. (2013). As we are not aware of a RCS matrix for RF explicitly calculated for the semi-direct effect, we use the average CO_2 and SO_2 coefficients shown in Shindell and Faluvegi (2010) based on Shindell and Faluvegi (2009). The semi-direct effect can potentially be included either in the response based on RCS values or in the RF. Our approach is to include the semi-direct effect in the RF and not in the RCS values; see next paragraph for details. The relationship for the deposition of BC on snow is also given by the CO_2 coefficients shown in Shindell and Faluvegi (2010). For the snow albedo effect, we have assumed an efficacy of 3 for all RF occurring outside of the Arctic (Myhre et al., 2013).

Our method differs from Shindell and Faluvegi (2009) as we have calculated the semi-direct effect independently. Since Shindell and Faluvegi (2009) did not have any rapid adjustments in their sensitivities on RFs, the rapid adjustments are implicitly included in their sensitivity coefficients. The reason is that in the GCM simulations used to calculate the forcing-response coefficients (Shindell and Faluvegi, 2009; Flanner, 2013), semi-direct effects are treated as feedbacks and as such they are included in the forcing-response coefficients. When we normalize to the global response to find the RCS coefficients, we normalize on the global CO_2

response given by Shindell and Faluvegi (2009) for all the species to avoid double counting.

2.2.4 Refinement of Arctic response to BC

We apply two refinements of the forcing-response coefficients for RFs occurring in the Arctic: one for the aerosol effects in the atmosphere and one for the effects due to BC on snow. We first discuss how we handle the aerosol effects in the atmosphere.

For BC in the Arctic, the forcing by absorption takes place in a generally stably stratified atmosphere (Quinn et al., 2008). The transport of BC to the Arctic occurs approximately along isentropic surfaces; thus emissions from East Asia are generally at a higher altitude than emissions from Europe. The BC particles also cause dimming at the surface. In the Arctic, heat is not easily mixed down to the surface. The efficacy of BC forcing depends highly on the altitude of the BC (Flanner, 2013; Lund et al., 2014; Sand et al., 2013). To account for this the RTP concept is modified for BC forcing in the Arctic. The contribution by RF exerted in the three latitude bands outside the Arctic-to-Arctic warming ($\mathrm{ARTP(ex\text{-}Arc)}_{\mathrm{BC},r,\mathrm{Arc},s}$) is calculated with the standard method using RTP coefficients from Shindell and Faluvegi (2010), as described in Sect. 2.2.3:

$$\mathrm{ARTP(ex-Arc)}_{\mathrm{BC},r,\mathrm{Arc},s}(H) = \sum_{l=1}^{3} \frac{F_{l,\mathrm{BC},r,s}}{E_{\mathrm{BC},r,s}} \times \mathrm{RCS}_{\mathrm{BC},l,\mathrm{Arc}} \times R_{\mathrm{T}}(H). \quad (6)$$

For the RF within the Arctic the response ($\mathrm{ARTP(Arc)}_{\mathrm{BC},r,\mathrm{Arc},s}$) is calculated according to Eq. (7) following the method presented in Lund et al. (2014):

$$\mathrm{ARTP(Arc)}_{\mathrm{BC},r,\mathrm{Arc},s}(H) = \sum_{z} \frac{F(z)_{\mathrm{Arc},\mathrm{BC},r,s}}{E_{\mathrm{BC},r,s}} \times \mathrm{RCS}(z)_{\mathrm{BC},\mathrm{Arc},\mathrm{Arc}} \times R_{\mathrm{T}}(H). \quad (7)$$

Both the RF ($F(z)_{\mathrm{Arc},\mathrm{BC},r,s}$) and the regional sensitivity matrix ($\mathrm{RCS}(z)_{\mathrm{BC},\mathrm{Arc},\mathrm{Arc}}$) have a dependence on the height of the BC, which is denoted by the z in Eq. (7). We apply a vertically resolved regional sensitivity matrix based on Fig. 2a in Lund et al. (2014), which shows the sensitivity of the Arctic surface temperature response to the altitude of RF in the Arctic from Flanner (2013) interpolated to the vertical structure in OsloCTM2. This relationship can be combined with the normalized BC RF from Samset and Myhre (2011) to give a normalized Arctic surface temperature response to BC perturbations at different altitudes.

We apply the vertical profile of BC concentration in the Arctic for all three models used. These vertical profiles are converted into RF profiles based on the vertically resolved RF to burden ratio in OsloCTM2.

Our second refinement is on the forcing-response coefficients for BC on snow in the Arctic, where we use the forcing-response sensitivity found by Flanner (2013).

As the semi-direct effect is implicitly included in the estimates for the BC aerosol effects for Arctic-to-Arctic warming from Flanner (2013), we cannot distinguish between direct RF and semi-direct RF for RF occurring in the Arctic. The Arctic RF, due to the semi-direct effect provided in Bellouin et al. (2016), is left out to avoid double counting. However, our argument is that the explicit vertically resolved forcing-response relationships is a much better fit than vertically averaged forcing-response relationships, which makes this the preferable method. As a result, this study's ARTP estimates of the semi-direct effect in the Arctic is due to the semi-direct RF from outside the Arctic.

The Flanner (2013) study is based on an equilibrium climate sensitivity of $0.91\,\mathrm{K\,m^2\,W^{-1}}$, which is 14 % lower than applied in our study. We adjust our calculations so that the climate sensitivity is in line with the rest of our calculations (Boucher and Reddy, 2008). The correction is done with a two-layer box-diffusion model based on the parameters of the Hadley Centre model (see Aamaas et al., 2013), which also modifies the timescales of the impulse response function.

The total response in the Arctic is then the sum of the contributions from BC forcing outside of the Arctic and inside of the Arctic.

$$\mathrm{ARTP}_{\mathrm{BC},r,\mathrm{Arc},s}(H) = \mathrm{ARTP(ex-Arc)}_{\mathrm{BC},r,\mathrm{Arc},s}(H) + \mathrm{ARTP(Arc)}_{\mathrm{BC},r,\mathrm{Arc},s}(H) \quad (8)$$

3 Results

3.1 ARTP values

3.1.1 Best estimates

Results for ARTP(20)

The best estimates of ARTP values for a time horizon of 20 years are presented in Fig. 1 for each of the four emission regions, the four response bands, plus the global mean, for all emitted species considered here. We provide values for other time horizons (10, 50, and 100 years) in the Sect. S2. The rationale for highlighting 20 years is that, if the focus is to be placed on the mitigation of SLCFs, then it is more appropriate to investigate climate impacts on short timescales. Results for continuous time horizons between 1 and 50 years are given in Sect. 3.1.5.

The uncertainties in Fig. 1 are given as a range following the differences in RFs estimated between the models. We acknowledge other uncertainties, such as for climate sensitivity, which are discussed in Sect. 3.4. The uncertainty is often larger than the variation between different emission regions, seasons, and responses in the latitude bands. However, we will show in Sect. 3.1.4 that the relative variations between the best estimates for individual species are often robust. As ARTP values for the shipping sector are based on only two

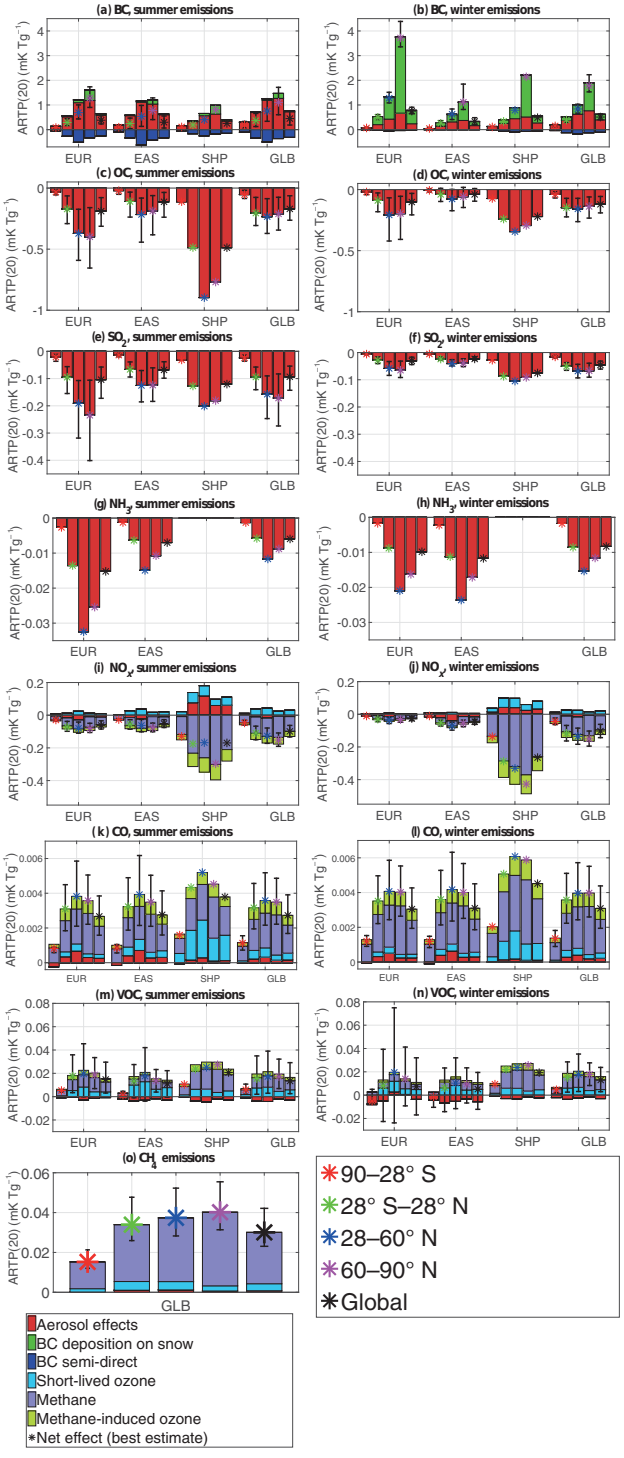

Figure 1. ARTP20 for emissions from Europe, East Asia, shipping, and global emissions for summer and winter. In each frame and for each emission region, the ARTP20 values for the four latitudinal response bands from south (left) to north (right), as well as the global response average (rightmost) for the species, are decomposed by effects. The net response is shown by the asterisk. The regions included are Europe (EUR), East Asia (EAS), shipping (SHP), and the globe (GLB), all for both NH summer, May–October (left), and NH winter, November–April (right). The uncertainty bars show the range across models, which is not given for shipping, as the best estimate is based on only two models for that sector. Due to the methodology applied, a fraction of the semi-direct effect for BC in the Arctic is included in the aerosol effects, as explained in Sect. 2.2.4. Note that the vertical axis varies between different emitted components.

RF estimates, uncertainty ranges are not given for shipping. The robustness in the best estimate for shipping is likewise lower than for other differences. These two models disagree for shipping on the sign for the aerosol effect of NO_x emissions. NH_3 estimates are also from one model only and are not shown for shipping (because emissions from that sector are negligible).

Response patterns

For emissions from a given region, the latitudinal response pattern is partly governed by the pattern of RF and partly by the pattern in the forcing-response coefficients. The RF signal is mainly located in the latitude bands near the emission sources for the short-lived constituents, while it is more evenly distributed for effects linked to methane. Hence, as shown in Bellouin et al. (2016; see their Fig. 7 in particular), emissions in Europe and East Asia give largest RF in the NH midlatitude band and the smallest in the Southern Hemisphere (SH) middle–high latitudes. Due mainly to heat transport between the latitude bands, the RCS coefficients also represent non-local temperature responses; thus, the temperature response is seen more evenly in all latitude bands. Nevertheless, the temperature response has higher sensitivity towards the Arctic and NH midlatitude bands (see all panels in Fig. 1) as a result of local feedback processes being stronger in the Arctic, driven by local cloud, water vapour, and surface albedo feedbacks (Boer and Yu, 2003).

We next consider differences between the emission regions Europe and East Asia. The RF per unit emission is dependent on where the emissions occur, which causes differences in the ARTP(20) values. The differences in the global average of RFs and global emission metric values such as AGTP(20) are discussed in Aamaas et al. (2016). In short, the emission metric values for the aerosols are larger for European than East Asian emissions, but not for NH_3 in winter. Variations are also seen for the ozone precursors, but these differences are relatively smaller for European than for East Asian emissions and for CO and VOC than for the aerosols. For CO, East Asia has marginally larger values than Europe (see Fig. 1k and l), while for VOC, European emissions have marginally larger values than for East Asian emissions (see Fig. 1m and n). The main difference between the global average of ARTP values calculated here and the AGTP values calculated in Aamaas et al. (2016) is the much larger impact for BC deposition on snow for ARTP (see Fig. 1b), as the AGTP study did not account for the increased efficacy of BC deposition on snow.

The timing of emissions also influences the RF per unit emissions. The emission metric values for the aerosol emissions in Europe and East Asia (see Fig. 1a–f) are larger for summer than for winter, except for BC. For the aerosols, the aerosol RF is driven by seasonal variations in the incoming solar radiation. More sunlight in local summer results in stronger RFs (Bellouin et al., 2016). Seasonal differences in atmospheric lifetimes due to seasonality in precipitation may also contribute. BC is discussed in detail in Sect. 3.1.2.

For the ozone precursors (see Fig. 1i–n), the largest values occur in winter for CO (Fig. 1l) and in summer for VOC (Fig. 1m). CO has a longer lifetime during local winter, leading to a larger fraction of the CO emitted being transported from the higher latitudes to the tropics. Here, the effects of CO oxidation on tropical OH have the largest impacts on the methane lifetime.

The latitudinal response patterns are similar for the different species. For all the species, the response bands with the largest ARTP values are for the responses in the NH midlatitudes (60 % of the cases) and Arctic, and the band with the least response is in the SH middle–high latitudes (see all panels in Fig. 1). This skewness towards the NH is partly due to the emissions occurring in the NH for Europe and East Asia, as well as mainly for the global emissions, but the same pattern is seen for CH_4 (Fig. 1o), for which the emission location is less important. Further, the high ARTP values for the Arctic are also due to stronger local feedback processes, leading to larger forcing-response sensitivities, while high ARTP values for the NH midlatitudes are a combination of high RF values per unit emission and relatively large regional climate sensitivities. Shindell et al. (2015) argue that the high responses in NH middle and high latitudes are not due to particular feedbacks for the SLCFs, but are mainly due to the efficacies driven by the large land fraction in this area and strong snow albedo feedbacks. The low ARTP values for SH middle–high latitudes are caused by a combination of the majority emissions occurring in NH for the emission regions and weaker forcing-response coefficients in SH. Let us consider OC emissions in East Asia during summer as an example with RF mostly in one band. The RF (see Bellouin et al., 2016) in the NH midlatitude band is 260 % above the global average, practically zero in the SH middle–high latitude band and about 50 % below the global average in the other two bands. This skewedness is also modelled in the ARTP (see Fig. 1c), but with more emphasis on the Arctic. The ARTP value for the responses in the Arctic and NH midlatitudes is about 70 and 90 % above the global average, respectively. In the SH middle–high latitude response band, the ARTP value is about 20 % of the global average. At the other end of the range, emissions of CH_4 have a global impact due to the atmospheric lifetime of CH_4 (9.7 years). The RF in the Arctic band is 35 % below the global average, but 25 % above in the tropics. However, the weighing is almost opposite for the ARTP, as the Arctic response band has a ARTP value 34 % above the global average and the tropics 13 % above the average (see Fig. 1o). For the SH middle–high latitude response band, both the RF and ARTP are lower than the global average, by −35 and −49 %, respectively.

For most of the aerosol emissions (see Fig. 1a–f), the ARTP values for the aerosol effects component are larger for emissions in NH summer than winter, even in the tropics for emission from both Europe and East Asia. The only excep-

tion is NH_3 (Fig. 1g and h), which has a larger ARTP value for winter than summer for East Asian and global emissions. Longer sunlight duration in the summer yields stronger RFs (Bellouin et al., 2016), which impact the ARTP value for the response even in the tropics. This general observation does not hold for BC when we include the effect "BC deposition on snow", as this effect is largest in NH winter, when the snow cover area is at its largest.

The ARTP(20) values shift sign for some of the latitude response bands. VOC emissions generally lead to warming, however, our best estimate indicates a small cooling in SH middle–high latitudes for European and East Asian winter emissions (Fig. 1n). The negative RF for the aerosol effect in this response band is driving this cooling, as the other perturbations have a small impact on the response in the SH middle–high latitudes. VOC emissions perturb aerosols via secondary organic aerosol formation, which two out of three models find to be cooling. For the ozone precursors, the aerosol effects, and the short-lived ozone effect to a smaller degree, also shift between warming and cooling depending on the latitude response band.

3.1.2 Variation of BC response with emission season and region

The largest differences in ARTP(20) values are seen for BC, such as the timing of emissions (comparing Fig. 1a and b), the location during winter (comparing the different emission regions in Fig. 1b), and response regions (comparing Arctic with other latitude bands for European emissions in Fig. 1b).

The total emission metric values of BC emissions depend on which effects are included. The direct aerosol effect is larger for summer than winter emissions. The direct temperature response is similar for emissions occurring in Europe, East Asia, and globally. Similarly, the semi-direct effect is most pronounced in summer as this effect is driven by absorption of shortwave radiation. When the influence from the BC deposition on snow is included, the ARTP value increases significantly for emissions during NH winter. For emissions in Europe, the global temperature response to the semi-direct effect is -46 and -12 % of the aerosol effect in summer and winter, respectively, and the effect of deposition on snow is 12 and 230 % of the aerosol effect in summer and winter, respectively. The relative share of the deposition on snow effect is 60 % lower for winter East Asian emissions than for winter European emissions. The semi-direct effect has a relative weight of -56 % compared to the aerosol effect for the global ARTP(20) East Asian emissions in summer and close to zero in winter. The impact of BC deposition on snow is largest when large snow- and ice-covered surface areas and solar radiation at the BC deposition location are combined, such as in late winter. The response from European emissions is larger than for East Asian emissions, since the emission region is closer to the Arctic, which makes BC transport into the sensitive Arctic more likely (Sand et al., 2013). The effect of the BC deposition on snow dominates the winter–summer difference for BC and hence our results are sensitive to both the calculated RF and efficacy for this BC process.

The Arctic response amplification (i.e. how much stronger the response is in the Arctic relative to the global average) is largest for winter emissions as the deposition on snow effect is relatively larger than for summer emissions. The total Arctic response amplification for BC is, for European emissions, 240 and 390 % larger than the global average in summer and winter, respectively, and for East Asian emissions 160 and 240 % larger. As a result, wintertime BC emissions have the largest latitudinal variation in the ARTP(20) among all SLCFs. This Arctic amplification is driven by the temperature response from deposition on snow effect (almost 500 % for European emissions and 400 % for East Asian emissions for this effect), which is largest in the Arctic response band, above the global average in the NH midlatitude, and below average in the two other response bands. Latitudinal response variations are also found for the other effects, but are relatively much smaller.

3.1.3 Comparison with Collins et al. (2013)

Our findings are largely consistent with those by Collins et al. (2013). Similarities occur because the two studies share some of the same forcing-response coefficients (Shindell and Faluvegi, 2009) and climate sensitivity (Boucher and Reddy, 2008). In this work, we have more detailed estimates for BC in the Arctic, and we include NH_3 as well as more detailed estimates for aerosol impacts on ozone precursors. ARTP values are also given for two seasons, for the shipping sector and our global estimate includes all emissions. The study by Collins et al. (2013) is more comprehensive than our study in terms of the number of models included, while the RF data set we use is newer and more detailed (see Table 1 in Bellouin et al., 2016), and the forcing-response coefficients are improved. Hence, results from both studies will be of benefit to those wanting to apply our metrics.

The ARTP(20) values in Collins et al. (2013) are mostly lower than the average response of annual emissions in this study, while the variations between the latitude response bands are mostly similar. We model 180 and 80 % stronger global temperature sensitivity from European and East Asian emissions of BC. The largest difference is that our study included the response from BC deposition in snow, whereas Collins et al. (2013) did not. In addition, Collins et al. (2013) applied a forcing-response coefficient for the BC direct RF that gives Arctic cooling due to emissions in the Arctic (Shindell and Faluvegi, 2009). When including a more detailed parameterization for atmospheric BC in the Arctic that considers the height of the BC (see Sect. 2.2.4), the global temperature response of BC emissions increases by 4–14 %. The difference is much larger in the Arctic, and the increase in the Arctic is 22–210 % when only considering the BC direct and first indirect effects.

3.1.4 Robustness for individual species

The differences between ARTP(20) values for different emission regions and emission seasons, as well as for the response in different latitude bands for one set of emissions, are smaller than the intermodel uncertainty ranges. However, the ARTPs based on RFs for the individual models agree often with the best estimate of the ranking between the different emission and response cases, which strengthens our confidence that the variations calculated for the best estimate are robust. In Sect. S3, we quantify this robustness and find a high robustness consistent with similar analysis done on AGTP(20) values (Aamaas et al., 2016). As the temperature response is more smeared out globally for the ozone precursors than for the aerosols, the models agree to a larger extent for the aerosols concerning which latitude response bands see the largest and smallest temperature perturbations. For BC, we compare results, only including the aerosol effects, as only one model includes BC on snow and semi-direct effects. The model NorESM has the largest discrepancy relative to the best estimate for NO_x and VOC, while HadGEM3 disagrees the most for CO.

3.1.5 Variations with time horizon

We have so far only analysed ARTP(20) values. Here we present results for a range of time horizons up to 50 years in Fig. 2. The ARTP values vary greatly with time horizon and generally decrease in magnitude with time for SLCFs, especially for the aerosols (see Fig. 2a and b for BC). The ranking between different regions, seasons, and latitude bands also changes with varying time horizon for the ozone precursors (see Fig. 2c–h). The reason is that the aerosols and aerosol precursors have atmospheric lifetimes of about a week, while methane has an atmospheric perturbation lifetime of almost 10 years, which will lead to variations in the relative weight of the short-term and long-term effects with varying time horizons for the ozone precursors (e.g. Collins et al., 2013).

The results show that NO_x emissions in Europe have in general more negative ARTP values for summer emissions than for winter emissions, which is due to a stronger methane effect (Fig. 2c). For East Asian emissions, the situation is mixed, with the most negative ARTP values in the first 10–15 years for winter emissions, while summer emissions have the most negative values for longer time horizons (Fig. 2d). For summer emissions, ARTP values in the first few years is pushed upwards by stronger solar insolation than in winter, leading to more short-lived ozone. For the ozone precursors, the ranking on which latitude band is the most sensitive is mostly unchanged after 5 years, but can vary in the first years.

3.2 Regional temperature response for 2008 emissions

Given the ARTP values, we calculate the regional and global temperature responses due to real-world emissions of SLCFs based on Eq. (2). The temperature response at time H in latitude band m for an emission E of species i is

$$\Delta T_{i,r,m,s}(H) = E_{i,r,s} \times \mathrm{ARTP}_{i,r,m,s}(H). \quad (9)$$

We estimate the temperature response in the four latitude bands for a time horizon of 20 years given real-world pulse emissions in 2008 from Europe, East Asia, the shipping sector, and globally (Klimont et al., 2017). The global emissions are given in Supplement Table S7. Such a view on regional responses is useful as regional variations will be hidden in the global mean response (e.g. Lund et al., 2012). The emissions include seasonal variability with emissions often being largest in the NH winter season. The temperature perturbations are mainly governed by the ARTP(20) values given in Sect. 3.1.1, but also by the seasonal cycle of the emissions. The emissions in Europe and East Asia are larger in winter than summer for all species except NH_3, driven by larger residential heating and cooking emissions during winter conditions. BC emissions are about 70 % larger in winter than in summer, OC emissions 70–100 % larger, and SO_2 emissions almost 20 % larger in East Asia and more than 40 % larger in Europe (Klimont et al., 2017). The seasonal variability is smaller for all the ozone precursors, with CO having the largest range among the ozone precursors (43 % more in winter).

For the global source region, ignoring the seasonality by applying annually averaged emissions and ARTP values gives similar total temperature responses to treating the seasons separately and then averaging (differences of 0–3 %). However, when treating Europe or East Asia individually seasonal information changes the temperature estimates by up to 18 %. The difference is largest for the aerosols. For Europe, the temperature response increases by 8 % for BC and decreases the cooling by OC by 10 %. The largest relative changes are seen in the net temperature perturbation of all SLCFs.

Figure 3 shows that the temperature perturbations are smallest for the SH middle–high response latitudes and largest for the Arctic and NH midlatitudes, as seen for ARTP(20). For most latitude response bands, SO_2 has the largest impact, so the net effect of the seven SLCFs is a cooling in most of the cases. BC has the second largest impact with a warming that is largest for winter emissions. The shipping sector is dominated by cooling from SO_2 and NO_x (see Fig. 3e and f), while the other sectors have a much broader mix of species causing both heating and cooling. However, NO_x can be both warming and cooling depending on emission metric choices. For ARTP(20) applying sustained emissions, NO_x has a relatively smaller cooling impact and even contributes to warming in some latitude bands for shipping emissions in summer (see Supplement Fig. S1).

Emission of non-CH_4 SLCFs leads normally to net cooling or effects that cancel each other out. However, we show that some specific cases cause warming in the Arctic (see Fig. 3b, d, and h). Winter emissions in Europe and East Asia cause

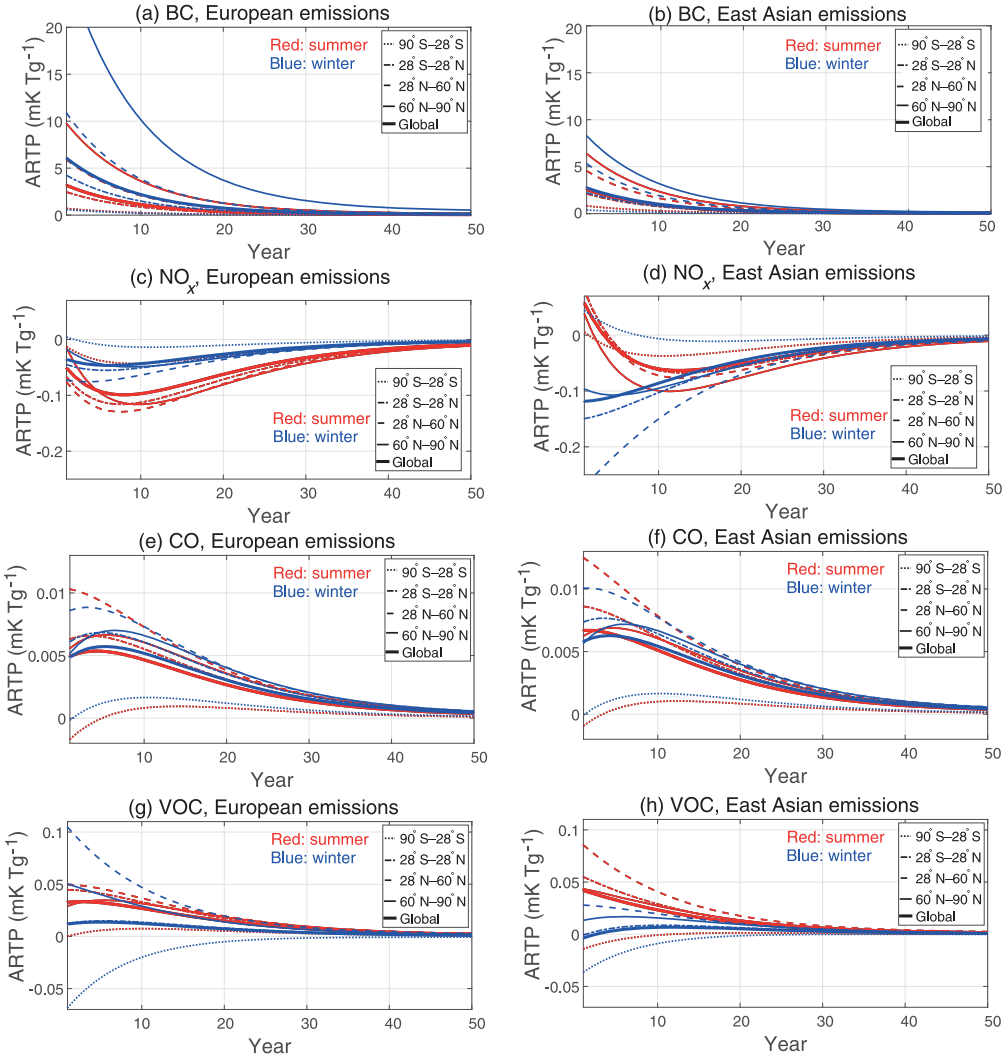

Figure 2. ARTP values in different response bands for BC and the ozone precursors for time horizons up to 50 years. Emissions in Europe (left) and East Asia (right) in NH summer (May–October) are given as red and in NH winter (November–April) as blue.

a warming in the Arctic and almost no net perturbation in the NH midlatitudes and other bands. The main reasons for the seasonality differences are the strong heating from the BC deposition on snow for winter emissions close to snow and ice surfaces, the relatively larger BC emissions in winter than for the other species, and weaker cooling effects of SO_2 in winter. For summer emissions in Europe and East Asia (Fig. 3a and c), the situation is the opposite with the largest cooling in the Arctic and NH midlatitudes. A small net heating in the Arctic is also observed for global emissions in the NH winter season.

3.3 Global temperature response and comparing ARTP and AGTP

We discuss how adding complexity with four latitudinal response bands impacts the metric value by comparing the global temperature response for regional and seasonal emissions presented in Sect. 3.2 based on ARTP with the AGTP calculation in Aamaas et al. (2016). Shindell (2014) concluded that the efficacy of the temperature response depends on the location of the RF. As a result, more RF in the NH middle to high latitudes for the aerosols gives a larger response than a globally averaged RF. Lund et al. (2012) found that an emission metric first based on regional variations, then averaged globally gives a more complete and informative value than one based on global mean inputs. Work by Stohl et al. (2015) shows that regional temperature estimates based on ARTPs mostly agree with calculations from earth system models. Although heterogeneity can be better included in temperature responses given by ARTPs compared to AGTPs, the superiority of ARTPs relative to AGTPs has not been tested thoroughly and confirmed. However, we ar-

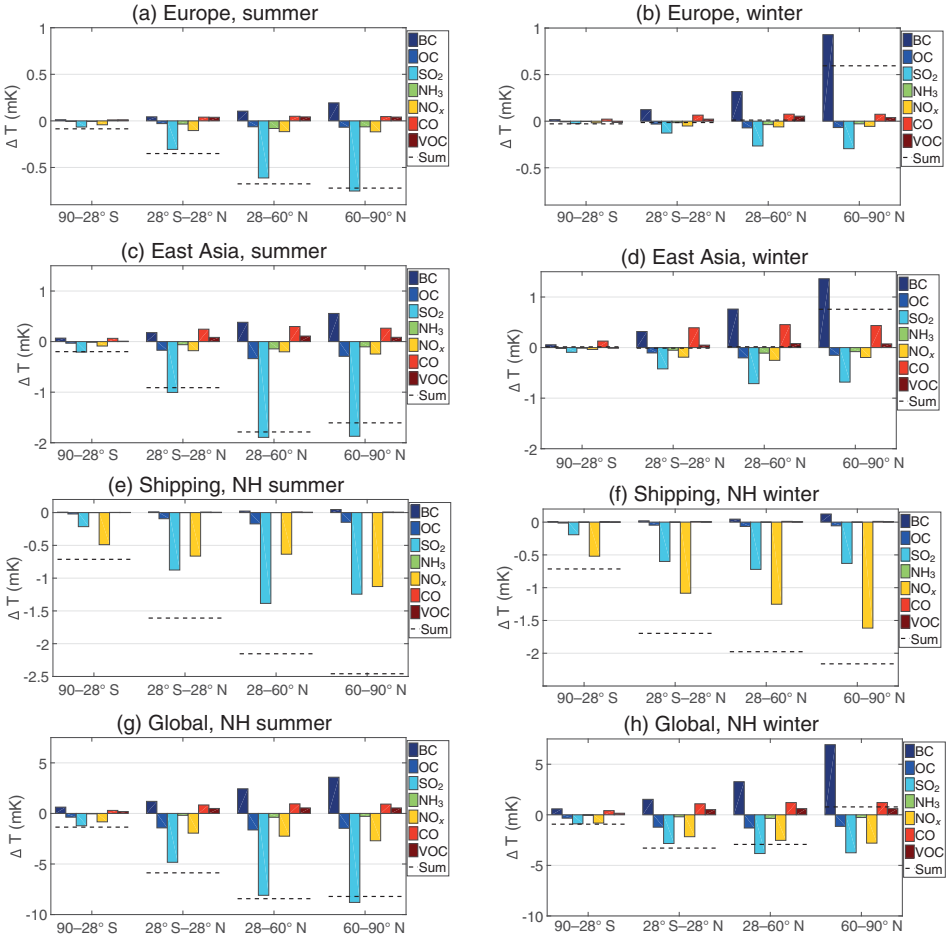

Figure 3. The regional temperature response for a time horizon of 20 years after regional and seasonal emissions in 2008 based on ARTP(20). The four latitude response bands represent the SH middle–high latitudes, tropics, NH midlatitudes, and Arctic. The global response average is given in Fig. S2. From top to bottom, the emission regions are Europe, East Asia, the global shipping sector, and the globe. The emissions are split into NH summer season (May–October) to the left and NH winter season (November–April) to the right. Note that the y axis differs for the regions. The horizontal dashed lines show the sum for each response band.

gue that the global temperature response can be better quantified with ARTPs than AGTPs, since a simple representation of varying efficacies due to heterogeneous RF is included.

How the global temperature responses are calculated given the AGTP values is shown in Sect. S6 and Aamaas et al. (2016). For the ARTP values, the global temperature is calculated from the area-weighted mean of the responses in the latitude bands. As the ARTP calculations are based on an efficacy of 3 for BC deposition on snow, the same efficacy is applied in the AGTP calculations. Our comparison between the methods applying ARTP and AGTP uses a pulse emission E. The difference in the global temperature perturbation ($\Delta T(\text{diff})$) for species i between the two methods is then

$$\Delta T(\text{diff})_{i,r,s}(H) = \sum_m E_{i,r,m,s} \times \text{ARTP}_{i,r,m,s}(H) - E_{i,r,s} \times \text{AGTP}_{i,r,s}(H), \quad (10)$$

which is applied for each emission region r and emission season s.

We compare the temperature perturbation based on ARTP and AGTP for a time horizon of 20 years using the 2008 emissions. The largest difference is for NH summer emissions. For global NH summer emissions, ARTP(20) results in 17 % more net cooling than AGTP(20) and about 26 and 32 % more cooling for European and East Asian emissions, respectively. The differences in responses are smaller for NH winter emissions. Annually, global emissions lead to a 13 % larger cooling based on ARTP than on AGTP. See Sect. S7 in the Supplement for further details. The differences emerge because the patterns of RF and efficacy are correlated, with highest RFs and highest efficacies in the northern midlatitudes and Arctic. Thus, the ARTPs are necessary to even obtain a global temperature response, since they account for these correlations.

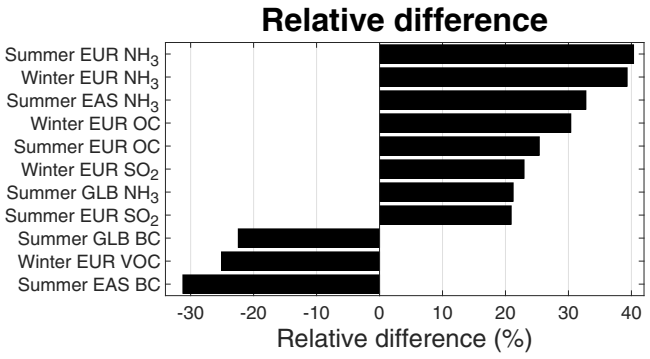

Figure 4. The relative difference between the global temperature responses based on ARTP and AGTP methods for a time horizon of 20 years. Only cases with larger relative differences than 20 % are shown. Positive numbers occur when the magnitude of the global temperature response is larger when based on ARTP than on AGTP, negative when the magnitude is largest based on AGTP.

Next, we analyse the differences between applying ARTP and AGTP for the individual species (see Figs. 4 and S3 in the Supplement). The relative differences are in most cases similar for the different emission regions and seasons for the same species, which show that the differences between ARTP and AGTP are governed by differences in the forcing-response coefficients between the two. The relative differences are generally larger for the aerosols than the ozone precursors, as seen in Fig. 4, where only the emissions regions and seasons with a relative difference larger than 20 % are presented. The temperature responses are generally stronger for the scattering aerosols and the BC deposition on snow given the ARTP than the AGTPs, which is in line with greater efficacies due to rapid and strong feedbacks for RFs in the northern midlatitudes and the Arctic latitude bands (Shindell, 2014). BC and ozone precursors are in general given lower weight when using ARTPs than when using AGTPs. Application of ARTP and AGTP values give variation of up to 30 % for individual effects, with an average of 12 % for individual species. ARTPs are more detailed in nature and through accounting for variations in efficacy will give more realistic global temperature responses.

3.4 Uncertainties

The ARTP values calculated have uncertainties and limitations given by the uncertainties in each parameter on the right-hand side of Eq. (1). The uncertainty ranges shown in Fig. 1 are based on the range in $\frac{F_{l,i}(t)}{E_i}$ across all contributing models. Bellouin et al. (2016) point out four important aspects regarding model diversity. Lifetime diversity is large, the unperturbed baseline causes diversity for non-linear mechanisms, the number of species included varies among the models, and finally the strength of the interactions between aerosols and chemistry differs among the models. The climate sensitivity included in R is 3.9 K for a doubling of CO_2 concentration (Boucher and Reddy, 2008); however, IPCC (2013) estimates the climate sensitivity to likely be in the range 1.5–4.5 K. Uncertainty is also found in the time evolution of R_T. We have based this impulse response function on only one model, while Olivié and Peters (2013) have shown that this will vary between models. For instance, they found a spread in the GTP(20) value of black carbon of about -60 to $+80$ % due to variability for R_T between models. However, the uncertainty in R_T is less relevant for the regional patterns. The forcing-response coefficients are also based mainly on one model (Shindell and Faluvegi, 2010). While we differentiate between emissions occurring during NH summer and winter season, forcing-response coefficients do not exist on a seasonal basis. Hence, the seasonal differences presented here in the ARTP values are not due to potential differences in the response sensitivities, but due to differences in the RF, Aamaas et al. (2016) observed that estimates of $\frac{F_{l,i}(t)}{E_i}$ tend to be correlated for different species in a model, which increases the uncertainty when a mitigation package is considered.

The temperature response will vary by species and location, such as between land surface and ocean surface. These differences are not accounted for in our study, but the increased efficacy in the RCS matrix towards the NH can be partly attributed to a larger land area fraction in the NH (Shindell et al., 2015). The temperature increase is in general larger over land than ocean (Boer, 2011) driven by several local feedbacks (Joshi et al., 2008). We do not have data to break down this effect for our emission regions, but results in Shindell (2012) indicate that the land response may be 20 % larger than the average.

More research is warranted to improve the temperature estimates and to reduce uncertainties. As the forcing-response coefficients (RCS) come mainly from one model, research is most needed to test the robustness of those model results, preferably in a multimodel intercomparison framework. We would also like to encourage work on how the temporal temperature response varies between the different latitude bands and species. As new data on RF from more and smaller emission regions are published in the future, and if RCS values become available for additional forcing and response regions, our study could be extended with this improved data.

The ARTP values are given for large emission regions, while large variations are likely within the regions. The impact of emissions from an European city may be very different to the average we have estimated for European emissions (see Bowman and Henze, 2012; Henze et al., 2012). They found that the key determinants for aerosols are the aerosol lifetime, surface albedo, and the chemical environment. Latitude is a key variable for ozone, but atmospheric chemistry, altitude, and vertical mixing play also a role.

Ideally, calculations of the temperature response of changed emissions of SLCFs should use earth system mod-

els for the most correct estimates. However, this is extremely time consuming, and many emission perturbations will have small signal-to-noise ratios. Users of emission metrics, such as policymakers and decision makers, might not have the needed expertise to utilize advanced models. Although the ARTP calculations are simplifications and contain uncertainties, these emission metrics are useful, simple, and quick approximations for calculating the temperature response in the different latitude bands for emissions of single species or a mix of SLCFs (and long-lived greenhouse gases).

4 Conclusions

We have presented ARTP values in four latitude bands (90–28° S, 28° S–28° N, 28–60° N, and 60–90° N) for several SLCFs (BC, OC, SO_2, NH_3, NO_x, CO, VOC, and CH_4) based on four different models. Numbers are provided for emission occurring in Europe, East Asia, and from the global shipping sector, as well as globally. Emissions were separated between the NH summer and winter seasons. Although ARTPs are simplifications, they are useful for analysing the temperature response to possible mitigation strategies. The ARTP values are largest in the response bands Arctic and NH midlatitudes and the smallest in the SH middle–high latitudes. The different models agree in most of the cases on the ranking of the temperature perturbation in the different latitude bands.

BC is the species that is the most sensitive to the timing of emissions and to the location during winter, as well as having the largest spread in responses between the latitude response bands in winter. The relative difference between the response bands is largest for BC emissions during NH winter and where emissions occur close to the Arctic. The Arctic temperature response is 390 and 240 % larger than the global temperature response for winter emissions in Europe and East Asia, respectively. BC deposition on snow is the most important effect that influences the Arctic for BC emissions occurring in NH winter, both in absolute and relative terms.

We have also investigated how the global response based on ARTP compares with AGTP. Our study indicates that the global temperature response can be better quantified with ARTPs than AGTPs, since ARTPs include a simple representation of varying efficacies due to heterogeneous RFs. For global emissions of SLCFs excluding CH_4, calculations based on ARTP values give 13 % larger cooling than when based on AGTP values. Globally, both these calculations based on ARTP(20) and AGTP(20) show a cooling, while European and East Asian winter emissions give a small net warming or near-zero impact according to ARTP. This is driven by net warming in the Arctic and close-to-zero perturbation in the other latitude bands. For summer emissions, net cooling occurs in all latitude bands, but are largest in the NH midlatitudes and Arctic. Seasonal emissions and seasonal ARTP values give almost the same total temperature response as annual emissions and annual ARTP values for global emissions, but change the temperature responses by up to 18 % when looking at emissions from individual regions such as Europe and East Asia.

Data availability. The RF data set used to calculate the emission metric values can be found in Bellouin et al. (2016).

The Supplement related to this article is available online at https://doi.org/10.5194/acp-17-10795-2017-supplement.

Competing interests. The authors declare that they have no conflict of interest.

Acknowledgements. The authors would like to acknowledge the support from the European Union Seventh Framework Programme (FP7/2007-2013) under grant agreement no 282688 – ECLIPSE, as well as funding by the Norwegian Research Council within the project "the Role of Short-Lived Climate Forcers in the Global Climate Regime" (project no. 235548). We thank Nicolas Bellouin for providing RF data for all the models. In addition, we show our appreciation to Nicolas Bellouin, Marianne Tronstad Lund, and Dirk Olivié for giving us vertical distributions of BC in the Arctic. We thank Daven K. Henze, Forrest Lacey, and three anonymous reviewers for valuable comments that were helpful for the paper. We also thank the editor for his contributions.

Edited by: Yves Balkanski
Reviewed by: four anonymous referees

References

Aamaas, B., Peters, G. P., and Fuglestvedt, J. S.: Simple emission metrics for climate impacts, Earth Syst. Dynam., 4, 145–170, https://doi.org/10.5194/esd-4-145-2013, 2013.

Aamaas, B., Berntsen, T. K., Fuglestvedt, J. S., Shine, K. P., and Bellouin, N.: Regional emission metrics for short-lived climate forcers from multiple models, Atmos. Chem. Phys., 16, 7451–7468, https://doi.org/10.5194/acp-16-7451-2016, 2016.

Bellouin, N., Baker, L., Hodnebrog, Ø., Oliviíe, D., Cherian, R., Macintosh, C., Samset, B., Esteve, A., Aamaas, B., Quaas, J., and Myhre, G.: Regional and seasonal radiative forcing by perturbations to aerosol and ozone precursor emissions, Atmos. Chem. Phys., 16, 13885–13910, https://doi.org/10.5194/acp-16-13885-2016, 2016.

Bentsen, M., Bethke, I., Debernard, J. B., Iversen, T., Kirkevåg, A., Seland, Ø., Drange, H., Roelandt, C., Seierstad, I. A., Hoose, C., and Kristjánsson, J. E.: The Norwegian Earth System Model, NorESM1-M – Part 1: Description and basic evaluation of the physical climate, Geosci. Model Dev., 6, 687–720, https://doi.org/10.5194/gmd-6-687-2013, 2013.

Boer, G. and Yu, B. Y.: Climate sensitivity and response, Clim. Dynam., 20, 415–429, https://doi.org/10.1007/s00382-002-0283-3, 2003.

Boer, G. J.: The ratio of land to ocean temperature change under global warming, Clim. Dynam., 37, 2253–2270, https://doi.org/10.1007/s00382-011-1112-3, 2011.

Boucher, O. and Reddy, M. S.: Climate trade-off between black carbon and carbon dioxide emissions, Energ. Policy, 36, 193–200, 2008.

Bowman, K. and Henze, D. K.: Attribution of direct ozone radiative forcing to spatially resolved emissions, Geophys. Res. Lett., 39, L22704, https://doi.org/10.1029/2012GL053274, 2012.

Cherubini, F., Fuglestvedt, J., Gasser, T., Reisinger, A., Cavalett, O., Huijbregts, M. A. J., Johansson, D. J. A., Jørgensen, S. V., Raugei, M., Schivley, G., Strømman, A. H., Tanaka, K., and Levasseur, A.: Bridging the gap between impact assessment methods and climate science, Environ. Sci. Policy, 64, 129–140, https://doi.org/10.1016/j.envsci.2016.06.019, 2016.

Collins, W. J., Fry, M. M., Yu, H., Fuglestvedt, J. S., Shindell, D. T., and West, J. J.: Global and regional temperature-change potentials for near-term climate forcers, Atmos. Chem. Phys., 13, 2471–2485, https://doi.org/10.5194/acp-13-2471-2013, 2013.

Flanner, M. G.: Arctic climate sensitivity to local black carbon, J. Geophys. Res.-Atmos., 118, 1840–1851, https://doi.org/10.1002/jgrd.50176, 2013.

Fry, M. M., Naik, V., West, J. J., Schwarzkopf, D., Fiore, A., Collins, W. J., Dentener, F., Shindell, D. T., Atherton, C. S., Bergmann, D. J., Duncan, B. N., Hess, P. G., MacKenzie, I. A., Marmer, E., Schultz, M. G., Szopa, S., Wild, O., and Zeng, G.: The influence of ozone precursor emissions from four world regions on tropospheric composition and radiative climate forcing, J. Geophys. Res., 117, D07306, https://doi.org/10.1029/2011JD017134, 2012.

Fuglestvedt, J. S., Berntsen, T. K., Godal, O., Sausen, R., Shine, K. P., and Skodvin, T.: Metrics of climate change: Assessing radiative forcing and emission indices, Climatic Change, 58, 267–331, 2003.

Fuglestvedt, J. S., Shine, K. P., Berntsen, T., Cook, J., Lee, D. S., Stenke, A., Skeie, R. B., Velders, G. J. M., and Waitz, I. A.: Transport impacts on atmosphere and climate: Metrics, Atmos. Environ., 44, 4648–4677, 2010.

Henze, D. K., Shindell, D. T., Akhtar, F., Spurr, R. J. D., Pinder, R. W., Loughlin, D., Kopacz, M., Singh, K., and Shim, C.: Spatially Refined Aerosol Direct Radiative Forcing Efficiencies, Environ. Sci. Technol., 46, 9511–9518, https://doi.org/10.1021/es301993s, 2012.

Hewitt, H. T., Copsey, D., Culverwell, I. D., Harris, C. M., Hill, R. S. R., Keen, A. B., McLaren, A. J., and Hunke, E. C.: Design and implementation of the infrastructure of HadGEM3: the next-generation Met Office climate modelling system, Geosci. Model Dev., 4, 223–253, https://doi.org/10.5194/gmd-4-223-2011, 2011.

IPCC: The Physical Science Basis. Contribution of Working Group I to the Fifth Assessment Report of the Intergovernmental Panel on Climate Change, edited by: Stocker, T. F., Qin, D., Plattner, G. K., Tignor, M., Allen, S. K., Boschung, J., Nauels, A., Xia, Y., Bex, V., and Midgley, P. M., Cambridge University Press, Cambridge, United Kingdom and New York, NY, USA, 1535 pp., 2013.

Iversen, T., Bentsen, M., Bethke, I., Debernard, J. B., Kirkevåg, A., Seland, Ø., Drange, H., Kristjansson, J. E., Medhaug, I., Sand, M., and Seierstad, I. A.: The Norwegian Earth System Model, NorESM1-M – Part 2: Climate response and scenario projections, Geosci. Model Dev., 6, 389–415, https://doi.org/10.5194/gmd-6-389-2013, 2013.

Joshi, M. M., Gregory, J. M., Webb, M. J., Sexton, D. M. H., and Johns, T. C.: Mechanisms for the land/sea warming contrast exhibited by simulations of climate change, Clim. Dynam.., 30, 455–465, https://doi.org/10.1007/s00382-007-0306-1, 2008.

Klimont, Z., Höglund-Isaksson, L., Heyes, C., Rafaj, P., Schöpp, W., Cofala, J., Purohit, P., Borken-Kleefeld, J., Kupiainen, K., Kiesewetter, G., Winiwarter, W., Amann, M., Zhao, B., Wang, S. X., Bertok, I., and Sander, R.: Global scenarios of air pollutants and methane: 1990–2050, in preparation, 2017.

Lund, M., Berntsen, T., Fuglestvedt, J., Ponater, M., and Shine, K.: How much information is lost by using global-mean climate metrics? an example using the transport sector, Climatic Change, 113, 949–963, https://doi.org/10.1007/s10584-011-0391-3, 2012.

Lund, M. T., Berntsen, T. K., Heyes, C., Klimont, Z., and Samset, B. H.: Global and regional climate impacts of black carbon and co-emitted species from the on-road diesel sector, Atmos. Environ., 98, 50–58, https://doi.org/10.1016/j.atmosenv.2014.08.033, 2014.

Myhre, G., Highwood, E., Shine, K. P., and Stordal, F.: New estimates of radiative forcing due to well mixed greenhouse gases, Geophys. Res. Lett., 25, 2715–2718, 1998.

Myhre, G., Berglen, T. F., Johnsrud, M., Hoyle, C. R., Berntsen, T. K., Christopher, S. A., Fahey, D. W., Isaksen, I. S. A., Jones, T. A., Kahn, R. A., Loeb, N., Quinn, P., Remer, L., Schwarz, J. P., and Yttri, K. E.: Modelled radiative forcing of the direct aerosol effect with multi-observation evaluation, Atmos. Chem. Phys., 9, 1365–1392, https://doi.org/10.5194/acp-9-1365-2009, 2009.

Myhre, G., Shindell, D., Bréon, F.-M., Collins, B., Fuglestvedt, J. S., Huang, J., Koch, D., Lamarque, J.-F., Lee, D., Mendoza, B., Nakajima, T., Robock, A., Stephens, G., Takemura, T., and Zhang, H.: Anthropogenic and Natural Radiative Forcing, in: Climate Change 2013: The Physical Science Basis. Contribution of Working Group I to the Fifth Assessment Report of the Intergovernmental Panel on Climate Change, edited by: Stocker, T. F., Qin, D., Plattner, G. K., Tignor, M., Allen, S. K., Boschung, J., Nauels, A., Xia, Y., Bex, V., and Midgley, P. M., Cambridge University Press, Cambridge, United Kingdom and New York, NY, USA, 2013.

Najafi, M. R., Zwiers, F. W., and Gillett, N. P.: Attribution of Arctic temperature change to greenhouse-gas and aerosol influences, Nature Clim. Change, 5, 246–249, https://doi.org/10.1038/nclimate2524, 2015.

Olivié, D. J. L. and Peters, G. P.: Variation in emission metrics due to variation in CO_2 and temperature impulse response functions, Earth Syst. Dynam., 4, 267–286, https://doi.org/10.5194/esd-4-267-2013, 2013.

Quinn, P. K., Bates, T. S., Baum, E., Doubleday, N., Fiore, A. M., Flanner, M., Fridlind, A., Garrett, T. J., Koch, D., Menon, S., Shindell, D., Stohl, A., and Warren, S. G.: Short-lived pollutants in the Arctic: their climate impact and possible mitigation strategies, Atmos. Chem. Phys., 8, 1723–1735, https://doi.org/10.5194/acp-8-1723-2008, 2008.

Samset, B. H. and Myhre, G.: Vertical dependence of black carbon, sulphate and biomass burning aerosol radiative forcing, Geophy. Res. Lett., 38, L24802, https://doi.org/10.1029/2011GL049697, 2011.

Sand, M., Berntsen, T. K., Seland, Ø., and Kristjánsson, J. E.: Arctic surface temperature change to emissions of black carbon within Arctic or midlatitudes, J. Geophys. Res.-Atmos., 118, 7788–7798, https://doi.org/10.1002/jgrd.50613, 2013.

Schmale, J., Shindell, D., von Schneidemesser, E., Chabay, I., and Lawrence, M.: Clean up our skies, Nature, 515, 335–337, 2014.

Shindell, D. and Faluvegi, G.: Climate response to regional radiative forcing during the twentieth century, Nat. Geosci., 2, 294–300, 2009.

Shindell, D. and Faluvegi, G.: The net climate impact of coal-fired power plant emissions, Atmos. Chem. Phys., 10, 3247–3260, https://doi.org/10.5194/acp-10-3247-2010, 2010.

Shindell, D., Schulz, M., Ming, Y., Takemura, T., Faluvegi, G., and Ramaswamy, V.: Spatial scales of climate response to inhomogeneous radiative forcing, J. Geophys. Res.-Atmos., 115, D19110, https://doi.org/10.1029/2010JD014108, 2010.

Shindell, D., Kuylenstierna, J. C. I., Vignati, E., van Dingenen, R., Amann, M., Klimont, Z., Anenberg, S. C., Muller, N., Janssens-Maenhout, G., Raes, F., Schwartz, J., Faluvegi, G., Pozzoli, L., Kupiainen, K., Höglund-Isaksson, L., Emberson, L., Streets, D., Ramanathan, V., Hicks, K., Oanh, N. T. K., Milly, G., Williams, M., Demkine, V., and Fowler, D.: Simultaneously Mitigating Near-Term Climate Change and Improving Human Health and Food Security, Science, 335, 183–189, https://doi.org/10.1126/science.1210026, 2012.

Shindell, D. T.: Evaluation of the absolute regional temperature potential, Atmos. Chem. Phys., 12, 7955–7960, https://doi.org/10.5194/acp-12-7955-2012, 2012.

Shindell, D. T.: Inhomogeneous forcing and transient climate sensitivity, Nature Clim. Change, 4, 274–277, https://doi.org/10.1038/nclimate2136, 2014.

Shindell, D. T., Faluvegi, G., Rotstayn, L., and Milly, G.: Spatial patterns of radiative forcing and surface temperature response, J. Geophys. Res.-Atmos., 120, 5385–5403, https://doi.org/10.1002/2014JD022752, 2015.

Shine, K. P., Fuglestvedt, J. S., Hailemariam, K., and Stuber, N.: Alternatives to the Global Warming Potential for Comparing Climate Impacts of Emissions of Greenhouse Gases, Climatic Change, 68, 281–302, https://doi.org/10.1007/s10584-005-1146-9, 2005.

Stevens, B., Giorgetta, M., Esch, M., Mauritsen, T., Crueger, T., Rast, S., Salzmann, M., Schmidt, H., Bader, J., Block, K., Brokopf, R., Fast, I., Kinne, S., Kornblueh, L., Lohmann, U., Pincus, R., Reichler, T., and Roeckner, E.: Atmospheric component of the MPI-M Earth System Model: ECHAM6, J. Adv. Model. Earth Syst., 5, 146–172, https://doi.org/10.1002/jame.20015, 2013.

Stohl, A., Aamaas, B., Amann, M., Baker, L. H., Bellouin, N., Berntsen, T. K., Boucher, O., Cherian, R., Collins, W., Daskalakis, N., Dusinska, M., Eckhardt, S., Fuglestvedt, J. S., Harju, M., Heyes, C., Hodnebrog, Ø., Hao, J., Im, U., Kanakidou, M., Klimont, Z., Kupiainen, K., Law, K. S., Lund, M. T., Maas, R., MacIntosh, C. R., Myhre, G., Myriokefalitakis, S., Olivié, D., Quaas, J., Quennehen, B., Raut, J.-C., Rumbold, S. T., Samset, B. H., Schulz, M., Seland, Ø., Shine, K. P., Skeie, R. B., Wang, S., Yttri, K. E., and Zhu, T.: Evaluating the climate and air quality impacts of short-lived pollutants, Atmos. Chem. Phys., 15, 10529–10566, https://doi.org/10.5194/acp-15-10529-2015, 2015.

Søvde, O. A., Gauss, M., Smyshlyaev, S. P., and Isaksen, I. S. A.: Evaluation of the chemical transport model Oslo CTM2 with focus on arctic winter ozone depletion, J. Geophys. Res.-Atmos., 113, D09304, https://doi.org/10.1029/2007JD009240, 2008.

Tol, R. S. J., Berntsen, T., O'Neill, B. C., Fuglestvedt, J. S., and Shine, K.: A unifying framework for metrics for aggregating the climate effect of different emissions, Environ. Res. Lett., 7, 044006, https://doi.org/10.1088/1748-9326/7/4/044006, 2012.